

# SuperMVS: Non-Uniform Cost Volume For High-Resolution Multi-View Stereo

Tao Zhang

atztao@gmail.com

## Abstract

Different from most state-of-the-art (SOTA) algorithms that use static and uniform sampling methods with a lot of hypothesis planes to get fine depth sampling. In this paper, we propose a **free-moving** hypothesis plane method for **dynamic and non-uniform** sampling in a wide depth range to build the cost volume, which not only greatly reduces the number of planes but also finers sampling, for both of reducing computational cost and improving accuracy, named **Non-Uniform Cost Volume**. We present the **SuperMVS** network to implement Multi-View Stereo with Non-Uniform Cost Volume. SuperMVS is a coarse-to-fine framework with four cascade stages. It can output higher resolution and accurate depth map. Our SuperMVS achieves the SOTA results with low memory, low runtime, and fewer planes on the DTU datasets and Tanks & Temples dataset.

## 1. Introduction

3D reconstruction from multiple images is one of the important problems in Computer Vision and Geometry. It is widely used in Autopilot, Smart City, Robot, and AR/VR. In the 3D reconstruction, Multi-view Stereo (MVS) is an indispensable step. It converts into a 3D model from multiple pictures and camera parameters. Recently, some MVS methods based on Deep Learning have also achieved good performance in 3D reconstruction.

Learning-based MVS algorithms [23] [9] [21] [22] [5], build the 3D Cost Volume to estimation depth. However, the 3D Cost Volume needs more planes subdivision the hypothesis range for higher precision depth sampling, leading to high memory and computational cost. Such as MVS-Net [23] and R-MVSNet [24] using 256 and 512 planes for sampling the depth, their large cost volume makes optimizations take much memory and runtime. Follow-up methods like CasMVSNet [9] and UCS-Net [23] use cascade architecture for coarse-to-fine the depth to reduce the number of planes to 48 and 64 planes. They can output a higher-resolution depth map with low memory and runtime. Therefore, reducing the number of planes is the key to reduce memory and runtime. However, how do we achieve higher

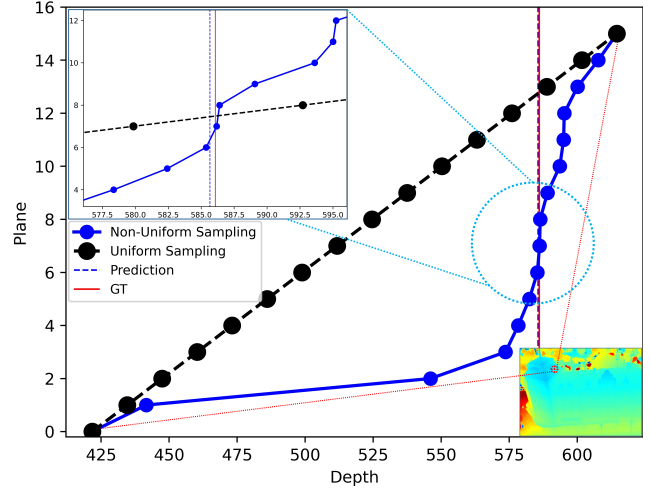


**Figure 1.** The figure shows the difference between the uniform sampling method and non-uniform sampling method. The interval between the hypothesis planes of uniform sampling is equal, but the non-uniform sampling changes dynamically. Our method can make most of the planes cluster around the ground truth. It provides more flexible and finer interval division.

accuracy with fewer planes?

In this paper, we propose a novel Non-Uniform Cost Volume method where plane moves *freely* in the depth range for *dynamic and non-uniform* sampling to build the cost volume. We notice that most algorithms use a uniform method for sampling, which require a sufficient number of planes to cover the entire depth range. The minimum depth units of uniform sampling  $\Delta d = \frac{\Delta R}{planes}$  depends on the number of *planes*, larger *planes* requiring to the higher fine sampling and more memory of cost volume  $h \times w \times planes$ . The CNNs do not have long-range attention. Most planes are redundant, which near the ground truth are valid. Our method is free to move most planes around the ground truth and make nearby sampling finer to achieve higher accuracy with a fewer number of planes. In Fig. 1, the interval between the plane of uniform sampling is static and uniform. But in our method, it is dynamic and non-uniform. Our method is more efficient than uniform sampling at the same number of planes, with a higher density of planes distributed around the ground truth.

We present the SuperMVS network with our Non-

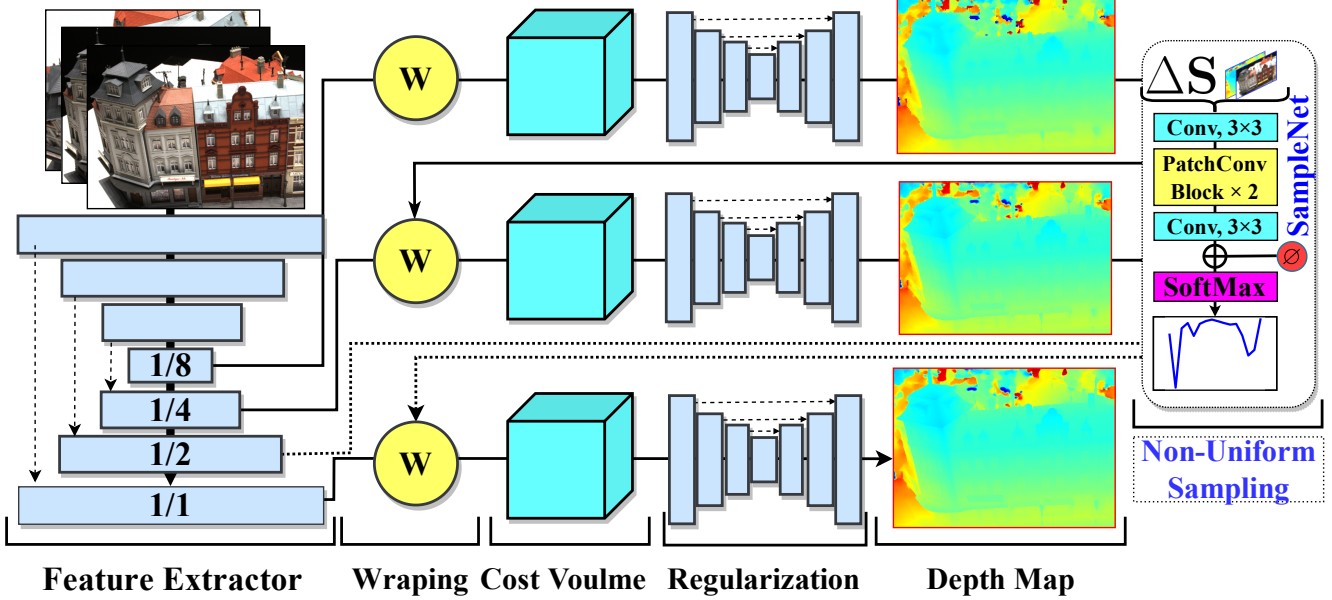


**Figure 2.** SuperMVS is a coarse-to-fine architecture with four cascade stages, to estimate a higher accurate depth. We use the U-Net to extract four feature maps of the  $\{\frac{H}{8} \times \frac{W}{8}, \frac{H}{4} \times \frac{W}{4}, \frac{H}{2} \times \frac{W}{2}, H \times W\}$  for coarse-to-fine the depth. All stages perform non-uniform sampling by the SampleNet to build the 3D cost volume, except that the first stage use the uniform sampling for initialize the depth.

Uniform Cost Volume method for Multi-View Stereo, which is a coarse-to-fine framework with four stages. To establish an efficient non-uniform sampling distribution, we propose SampleNet in the SuperMVS. The SampleNet makes the plane move freely in a wide depth sampling range to predict more accurate sampling. SuperMVS can output high resolution and high precision depth maps with low memory and runtime compared with other algorithms. We also achieve the state-of-the-art result on the DTU dataset [1] and Tanks & Temples dataset [14].

## 2. Method

Fig.2 shows the architecture of SuperMVS. In this section, we describe the forward propagation process of SuperMVS. In Sec. 2.1, we introduce the multi-scale cascade structure for feature extraction. In Sec. 2.2, we build non-uniform cost volume with the non-uniform sampling. In Sec. 2.3, we talk about how to regularize the non-uniform cost volume by 3D CNN to predict the depth and loss function.

The task of SuperMVS is to input  $N$  images and camera parameters, and output the depth map  $\hat{L}_k$ . For simplicity, denote reference image  $\mathbf{I}_1$ , source images  $\{\mathbf{I}_i\}_{i=2}^N$ , and camera intrinsic and extrinsic matrices  $\{K_i, T_i\}_{i=1}^N$ .

### 2.1. Feature Extraction

This module is to extract  $N$  images as feature maps  $\{F_{1,i}, F_{2,i}, F_{3,i}, F_{4,i}\}$  with the resolution of  $\frac{H}{8} \times \frac{W}{8}, \frac{H}{4} \times \frac{W}{4}, \frac{H}{2} \times \frac{W}{2}$  and  $H \times W$ . We build a multi-scale feature extraction module based on U-Net [17], which includes the

part of encoder and decoder. The encoder uses stride 2 convolution for downsampling, and the decoder uses stride 2 deconvolution for upsampling. Each convolution or deconvolution is followed by BN [11] and ReLU [2]. The low-scale features from the encoder are merged by the concatenation operation. The multi-scale feature extraction structure not only extracts more advanced features, but also reduces computational consumption. By fusing features of different scales in the decoder part, the redundant features can be reduced, thereby capturing more detailed features. In our model, the channels of four stage  $\{C_1, C_2, C_3, C_4\}$  are  $\{64, 32, 16, 8\}$ .

### 2.2. Non-Uniform Cost Volume

**Homography Wrapping.** We use differentiable homography warping, from the feature map  $\{F_{1,i}, F_{2,i}, F_{3,i}, F_{4,i}\}_{i=2}^N$  of source views warping to the feature map  $\{F_{1,1}, F_{2,1}, F_{3,1}, F_{4,1}\}$  of the reference view, to construct the cost volume. The coordinate mapping relationship between different views is determined by homography:

$$H_i(d) = K_i T_i T_1^{-1} K_1^{-1} \quad (1)$$

We can find the pixel coordinate  $(x, y)$  and depth  $d$  of the reference views between each source view by the homography.

**Non-Uniform Sampling.** Assume that the depth range is  $[d_{min}, d_{max}]$ , the maximum depth sampling range is  $\Delta R = |d_{max} - d_{min}|$ . The number of hypothesis planes for sampling in hypothesis range  $\Delta R_k$  at  $k$ -th stage is  $D_k$ ,

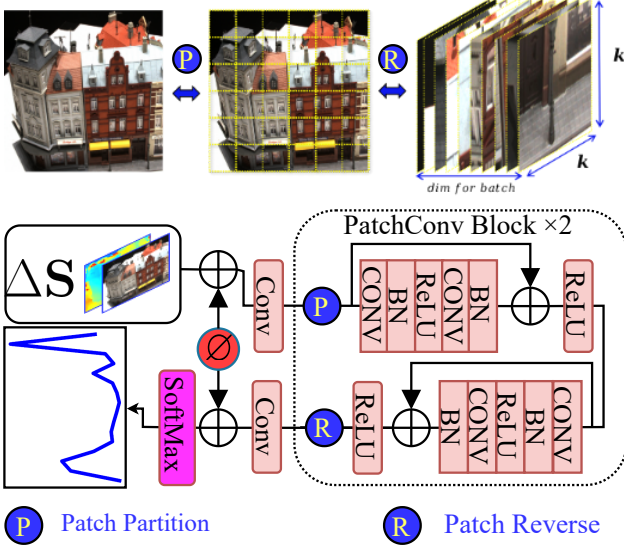


Figure 3. SampleNet with two PatchConv blocks.

$k \in \{1, 2, 3, 4\}$ . By the coarse-to-fine, when the depth is more accurate, the sampling range should be reduced. Hence we define a scale  $R_k$  ( $0 \leq R_k \leq 1$ ) for the hypothesis range  $\Delta R_k = R_k \Delta R$ .

For simplicity, we transform the sampling problem into a probability distribution problem. We purpose a SampleNet  $\mathcal{F}$  to predict the non-uniform sampling distribution with learning:

$$P_k = \mathcal{F}(\Delta \mathbf{S}_{k-1}, \hat{\mathbf{L}}_{k-1}, \mathbf{I}_1), \quad (2)$$

where  $\mathbf{I}_1$  is the reference view,  $\hat{\mathbf{L}}_{k-1}$  is the depth map of previous stage. We define the Sample Cost  $\Delta \mathbf{S}_{k-1}$  to quantify the quality of sampling at the previous stage and constrain the distribution of sampling at the next stage, which is calculated from the normalized standard deviation:

$$\Delta \mathbf{S}_{k-1} = \frac{e^{\sqrt{(\mathbf{L}_{k-1} - \hat{\mathbf{L}}_{k-1})^2 \cdot \mathbf{P}_{k-1}}}}{\sum_{j=0}^{D_{k-1}} e^{\sqrt{(\mathbf{L}_{k-1,j} - \hat{\mathbf{L}}_{k-1,j})^2 \cdot \mathbf{P}_{k-1,j}}}}. \quad (3)$$

When the standard deviation  $\sqrt{(\mathbf{L}_{k-1} - \hat{\mathbf{L}}_{k-1})^2 \cdot \mathbf{P}_{k-1}}$  limit to 0, it means that all planes are distributed around the depth maps  $\hat{\mathbf{L}}_{k-1}$ . The depth map  $\mathbf{L}_{k-1}$  and reference view  $\mathbf{I}_1$  can also regularize the sampling distribution. In our experiments, SampleNet can well couple the relationship between them. There is difference in the contribution to the accuracy,  $\Delta \mathbf{S}_{k-1}$  and  $\mathbf{L}_{k-1}$  contributes the most. It will be discussed in Sec. 3.4.

From the sampling distribution  $P_k$ , we have all the interval between the plane  $\Delta d_k$ :

$$\Delta d_k = P_k \cdot \Delta R_k, \quad (4)$$

and the sampling depth of  $j$ -th plane  $\mathbf{L}_{k,j}$  based on the pre-

vious estimate is:

$$\mathbf{L}_{k,j} = \hat{\mathbf{L}}_{k-1} - \frac{\sum_{j=0}^{D_k/2-1} \Delta d_{k,j} + \sum_{j=0}^{D_k/2} \Delta d_{k,j}}{2} + \sum_{j=0}^j \Delta d_{k,j} \quad \text{for } j = 0, 1, \dots, D_k. \quad (5)$$

Specially,  $-\frac{\sum_{j=0}^{D_k/2-1} \Delta d_{k,j} + \sum_{j=0}^{D_k/2} \Delta d_{k,j}}{2}$  makes the previous depth in the center of all planes which is important for coarse-to-fine at next stage and training.

**SampleNet With Image Patches.** SampleNet (See Fig.3) uses the two PatchConv blocks, which consists of two residual blocks [10] with inputting the image patches. Why do we use patches as input in SampleNet? We have tried CNN, MLP and Swin Transformer [15] as the SampleNet, but the performance of CNN and MLP is not so good as that of the Swin Transformer. The planes of CNN and MLP are distributed at both ends of the depth range. Only Swin Transformer satisfies our distribution requirements, which is distributed around the ground truth. We guess it is because the input of the Swin Transformer is the image patches. The Swin Transformer is too heavy, and we replace its window attention modules by convolution, which greatly improves the performance. There is no good global sampling distribution for whole input, but there is a better local distribution on local patches. In our experiments, we set the patches size to 8 and the channels to 32 in the SampleNet. We also add position encoding  $\emptyset$  to the input and output to represent hypothesis planes at different positions. Because the input is the patches, the sampling module is extremely low in computation and runtime, which is discussed in Sec. 3.4.

**Non-Uniform Cost Volume.** We get the depth  $\mathbf{L}_{k,j}$  of the reference view by the non-uniform sample. Then the depth  $d$  of pixel coordinates  $(x, y)$  is  $\mathbf{L}_{k,j}(x, y)$ , using the homography  $H_i(d)$  to wrap the feature map  $F_{i,k}$  of the multiple source views, build the non-uniform cost volume  $\Delta \mathbf{C}_{k,j}$ .

### 2.3. Depth Map and Loss Function

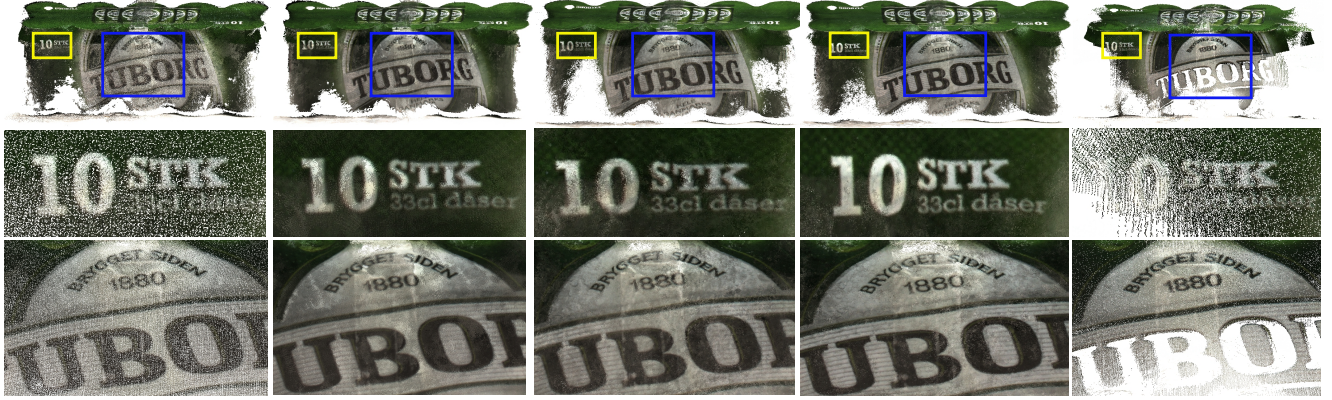
The 3D CNN is U-Net with the 3D convolution, but the skip connections are added. In the encoder, we downsample the input resolution from  $H \times W$  to  $\frac{H}{8} \times \frac{W}{8}$  and the decoder back to the input resolution by upsampling. The output layers, followed by SoftMax, output the depth probability  $\mathbf{P}_{k,j}$ .

We use the 3D CNN to regularize the 3D cost volume  $\Delta \mathbf{C}_{k,j}$  to get the depth probability  $\mathbf{P}_{k,j}$ . The depth map  $\hat{\mathbf{L}}_k$  of  $k$ -th stage is:

$$\hat{\mathbf{L}}_k = \sum_j \mathbf{L}_{k,j} \cdot \mathbf{P}_{k,j}. \quad (6)$$

For supervised learning our SuperMVS, we use four





a) R-MVSNet

b) CasMVSNet

c) UCS-Net

d) Ours

e) GT

**Figure 4.** Capture form the *Scan12* of the DTU testing dataset. We use some details to reflect the density of the reconstruction and the quality of the point cloud. Our method’s surface of the point cloud is less noisy and clearer.

smooth L1 losses [8] to build the loss function:

$$\mathcal{L} = \sum_{k=1}^{N=4} \lambda_k \cdot \text{smooth}_{L1}(\hat{L}_k - L_k^{gt}), \quad (7)$$

where  $\lambda_1 = 0.25$ ,  $\lambda_2 = 0.5$ ,  $\lambda_3 = 1$ ,  $\lambda_4 = 2$  and the  $L_k^{gt}$  is the ground truth of  $k$ -th stage.

### 3. Experiments

We evaluate our method on DTU and Tanks & Temples datasets. And Compare it with other state-of-the-art algorithms at performance, memory and runtime. We also discuss the contribution of the Non-Uniform Cost Volume to the model.

#### 3.1. Datasets

The DTU dataset [1] is a large-scale indoor MVS dataset with 124 different scenes. It includes images with different views and lighting, camera parameters and depth maps. It also provides the 3D point cloud data for all scenes. We use it to train, test and validation the model. The dataset split is the same as that in other methods defined at [12]. The Tanks & Temples dataset [14] consists of realistic indoor and outdoor scenes. It divided intermediate and advanced datasets. In our work, we train the SuperMVS on DTU training set, then test it on the DTU evaluation set and the intermediate set of Tanks & Temples dataset.

#### 3.2. Implementation

We set the images resolution to  $[H = 512, W = 640]$  and the number of input images to  $N = 5$ . The number of hypothesis plane is  $D_1 = 48$ ,  $D_2 = 16$ ,  $D_3 = 8$  and  $D_4 = 8$ . The scale of hypothesis range is  $R_2 = 0.38$ ,  $R_3 = 0.16$  and  $R_4 = 0.04$ . All stages use our non-uniform sampling method to build the cost volume, except for the first stage use the uniform sampling at  $\Delta R$  for initialize the

depth. We implement our model with Pytorch [16] and train it on  $2 \times$  Nvidia RTX 3090 GPUs with batch size of 4 per GPU. We employ the Adam [13] optimizer with an initial learning rate 0.0016 to train for 26 epoch, where the learning rate shcedule is divided by 2 every two epochs starting from  $10^{th}$  epoch.

#### 3.3. Benchmark Performance

Method	Acc.(mm)	Comp.(mm)	Overall.(mm)	Mem.(GB)	Runtime.(s)	Planes.
Geometric	Furi [6]	0.613	0.941	0.777	-	-
	Tola [20]	0.342	1.190	0.766	-	-
	Camp [3]	0.835	0.554	0.695	-	-
	Gipuma [7]	<b>0.283</b>	0.873	0.578	-	-
	Colmap [18] [19]	0.400	0.664	0.532	-	-
	SurfaceNet [12]	0.450	1.040	0.745	-	-
Learning	MVSNet [23]	0.396	0.527	0.462	>8	256
	R-MVSNet [24]	0.383	0.452	0.417	6.7	3.72
	Point-MVSNet [4]	0.342	0.411	0.376	>8	96
	Fast-MVSNet [25]	0.336	0.403	0.370	-	96
	CasMVSNet [9]	0.325	0.385	0.355	6.6	0.76
	CVP-MVSNet [22]	0.296	0.406	0.351	>8	96
	UCS-Net [5]	0.338	0.349	0.344	6.9	0.84
	Ours	0.359	<b>0.293</b>	<b>0.325</b>	<b>5.4</b>	<b>0.51</b>

**Table 1.** Quantitative results on DTU’s evaluation set [1] (lower is better).

**Evaluation on the DTU dataset.** We evaluate our method on the DTU testing set. The resolution of input images is  $[H = 1152, W = 1600]$  and the depth range is  $[425mm, 935mm]$ . The resolution of output depth map is equal to input. We reconstruct the point cloud by fusing the depth, to calculate the *accuracy*, *completeness* and *overall* metrics by the MATLAB evaluate code sourced from the DTU dataset. For a fair comparison, the GPU *Mem* and *Runtime* of all methods are run on Nvidia RTX 3070 with 8GB.

We compare our results with other state-of-the-art of learning-based methods as the baseline in Table.1. It is worth noting that most of them use the uniform sampling method in the table. Our method outperforms other algorithms on *completeness* and *overall*. We also list the number of planes set by different algorithms when the cost volume resolution is  $\frac{H}{4} \times \frac{W}{4} \times \text{planes}$ . We can see that the number of planes directly affects the accuracy, memory and

Method	Mean	Family	Francis	Horse	Lighthouse	M60	Panther	Playground	Train
MVSNet [23]	43.48	55.99	28.55	25.07	50.79	53.96	50.86	47.90	34.69
Fast-MVSNet [25]	47.39	65.18	39.59	34.98	47.81	49.16	46.20	53.27	42.91
Point-MVSNet [4]	48.27	61.79	41.15	34.20	50.79	51.97	50.85	52.38	43.06
R-MVSNet [24]	48.40	69.96	46.65	32.59	42.95	51.88	48.80	52.00	42.38
PatchmatchNet [21]	53.15	66.99	52.64	43.24	54.87	52.87	49.54	54.21	50.81
CVP-MVSNet [22]	54.03	76.50	47.74	36.34	55.12	<b>57.28</b>	<b>54.28</b>	57.43	47.54
UCS-Net [5]	54.83	76.09	53.16	43.03	54.00	55.60	51.49	57.38	47.89
CasMVSNet [9]	<b>56.42</b>	<b>76.36</b>	<b>58.45</b>	<b>46.20</b>	55.53	56.11	54.02	<b>58.17</b>	46.56
Ours	55.38	73.75	54.19	45.19	<b>56.90</b>	56.39	52.51	55.36	<b>48.78</b>

**Table 2.** Quantitative results of F-scores (higher means better) on Tanks & Temples.

runtime based on the uniform sampling method. Our model reduces computation and achieves competitive performance by using the least number of planes 16. Compared with R-MVSNet [24], large number of planes 512 leads to longer runtime 3.72s, our method reduces by 3.50s. Compared with UCS-Net [5], the number of planes 64 needs 6.9GB more memory, our method reduces the memory by 1.5GB. Our method also achieves significant improvement in *overall*, comparing to CasMVSNet [9] and UCS-Net, improving up 0.030mm and 0.019mm, respectively. In Fig. 4, we compare the qualitative of point cloud with R-MVSNet, CasMVSNet and UCS-Net. Our method has less noise and higher completeness.

**Evaluation on Tanks & Temples Dataset.** We also evaluate our model on the Tanks & Temples dataset, which is trained on the DTU dataset without any fine-tuning. We use the image size  $[H_{max} = 1024, W_{max} = 2048]$  and the number of views  $N = 10$  for input. The GPU memory and runtime spent on RTX Nvidia 3070 (8GB) are 6.5GB and 0.88s, respectively. We compare the F-scores of different published learning-based methods in Table. 2. Our method outperforms most algorithms, although belows CasMVSNet in the best average F-score, our speed and memory are superior, and we achieve the best F-scores on the Lighthouse and Train scene.

### 3.4. Ablation study

$N$	US	NUS	Acc.(mm)	Comp.(mm)	Overall.(mm)	Mem.(GB)	Runtime.(s)
5	✓		0.365	0.314	0.339	5.41	0.43
5		✓	<b>0.357</b> $\uparrow$ 0.012	0.300 $\uparrow$ 0.014	0.329 $\uparrow$ 0.010	5.41	0.45
6		✓	<b>0.357</b> $\uparrow$ 0.000	<b>0.293</b> $\uparrow$ 0.007	<b>0.325</b> $\uparrow$ 0.004	5.44	0.51
7		✓	0.359 $\downarrow$ 0.002	0.296 $\downarrow$ 0.003	0.327 $\downarrow$ 0.002	5.46	0.57

**Table 3.** Quantitative results on DTU’s evaluation set [1] with the number of input views  $N$ . We training our model with uniform sampling (US) method and non-uniform sampling (NUS) method.

**Number of Views.** We evaluate the DTU’s dataset with the different number of views  $N$ . The results are shown in Table. 3. As  $N$  increases, the performance will reach saturation. When  $N = 6$ , the performance is the best.

$I_1$	$L_{k-1}$	$\Delta S_{k-1}$	Acc.(mm)	Comp.(mm)	Overall.(mm)
✓	✓	✓	0.317	0.237	0.277
	✓	✓	0.322 $\downarrow$ 0.005	0.238 $\downarrow$ 0.001	0.280 $\downarrow$ 0.003
		✓	0.359 $\downarrow$ 0.042	0.276 $\downarrow$ 0.039	0.318 $\downarrow$ 0.041
	✓		0.381 $\downarrow$ 0.064	0.271 $\downarrow$ 0.034	0.326 $\downarrow$ 0.049
✓			1.792 $\downarrow$ 1.475	1.173 $\downarrow$ 0.936	1.483 $\downarrow$ 1.206

**Table 4.** Quantitative results on the Scan9 of DTU’s evaluation set [1] with the different input of SampleNet.

**Non-uniform Sampling Vs. Uniform Sampling.** In order to fully illustrate the superiority of our non-uniform sampling (NUS) method, we replace it in SuperMVS with uniform sampling (US), train with the same training strategy as the baseline. Table. 4 shows that the precision of our method (NUS) is better than the US, and this verifies the effectiveness of NUS. It should be pointed out that our SuperMVS can still outperform UCS-Net and CasMVSNet without NUS at *completeness* and *overall*. Comparing memory and runtime between them, we can also find that our SampleNet occupies almost negligible memory and runtime, and the running time is 20ms.

**Input Contribution.** Table. 3 shows the effect of different inputs on accuracy in SampleNet. The reference view  $I_1$  has the least impact on accuracy. The Sample Cost  $\Delta S_{k-1}$  and the depth map  $L_{k-1}$  have the greatest impact on accuracy. It shows that they are necessary to establish the correct sampling distribution.

## 4. Conclusion

This paper presents a novel dynamic and non-uniform sampling method with fewer free-moving planes for 3D cost volume. We build the SuperMVS for Multi-View Stereo to achieve the purpose of low memory, low runtime and higher accuracy. We achieve the state-of-the-art performance on multiple datasets to verify our method’s effectiveness. In the future, we plan to extend the method for other applications and combine position encoding with 2D convolution instead of 3D convolution regularization for the 3D Cost Volume.

## References

- [1] Henrik Aanaes, Rasmus Ramsbøl Jensen, George Vogiatzis, Engin Tola, and Anders Bjarholm Dahl. Large-scale data for multiple-view stereopsis. *Int. J. Comput. Vis.*, 120(2):153–168, 2016. 2, 4, 5
- [2] Abien Fred Agarap. Deep learning using rectified linear units (relu), 2018. cite arxiv:1803.08375Comment: 7 pages, 11 figures, 9 tables. 2
- [3] Neill D. F. Campbell, George Vogiatzis, Carlos Hernández, and Roberto Cipolla. Using multiple hypotheses to improve depth-maps for multi-view stereo. In David A. Forsyth, Philip H. S. Torr, and Andrew Zisserman, editors, *ECCV (1)*, volume 5302 of *Lecture Notes in Computer Science*, pages 766–779. Springer, 2008. 4
- [4] Rui Chen, Songfang Han, Jing Xu, and Hao Su. Point-based multi-view stereo network. In *ICCV*, pages 1538–1547. IEEE, 2019. 4, 5
- [5] Shuo Cheng, Zexiang Xu, Shilin Zhu, Zhuwen Li, Li Erran Li, Ravi Ramamoorthi, and Hao Su. Deep stereo using adaptive thin volume representation with uncertainty awareness. In *CVPR*, pages 2521–2531. IEEE, 2020. 1, 4, 5
- [6] Yasutaka Furukawa and Jean Ponce. Accurate, dense, and robust multiview stereopsis. *IEEE Trans. Pattern Anal. Mach. Intell.*, 32(8):1362–1376, 2010. 4
- [7] Silvano Galliani, Katrin Lasinger, and Konrad Schindler. Massively parallel multiview stereopsis by surface normal diffusion. In *ICCV*, pages 873–881. IEEE Computer Society, 2015. 4
- [8] Ross Girshick. Fast r-cnn, 2015. cite arxiv:1504.08083Comment: To appear in ICCV 2015. 4
- [9] Xiaodong Gu, Zhiwen Fan, Siyu Zhu, Zuozhuo Dai, Feitong Tan, and Ping Tan. Cascade cost volume for high-resolution multi-view stereo and stereo matching. In *CVPR*, pages 2492–2501. IEEE, 2020. 1, 4, 5
- [10] Kaifeng He, Xiangyu Zhang, Shaoqing Ren, and Jian Sun. Deep residual learning for image recognition, 2015. cite arxiv:1512.03385Comment: Tech report. 3
- [11] Sergey Ioffe and Christian Szegedy. Batch normalization: Accelerating deep network training by reducing internal covariate shift. *arXiv preprint arxiv:1502.03167*, 2015. 2
- [12] Mengqi Ji, Juergen Gall, Haitian Zheng, Yebin Liu, and Lu Fang. Surfacenet: An end-to-end 3d neural network for multiview stereopsis. In *ICCV*, pages 2326–2334. IEEE Computer Society, 2017. 4
- [13] Diederik P Kingma and Jimmy Ba. Adam: A method for stochastic optimization. *arXiv preprint arXiv:1412.6980*, 2014. 4
- [14] Arno Knapitsch, Jaesik Park, Qian-Yi Zhou, and Vladlen Koltun. Tanks and temples: benchmarking large-scale scene reconstruction. *ACM Trans. Graph.*, 36(4):78:1–78:13, 2017. 2, 4
- [15] Ze Liu, Yutong Lin, Yue Cao, Han Hu, Yixuan Wei, Zheng Zhang, Stephen Lin, and Baining Guo. Swin transformer: Hierarchical vision transformer using shifted windows, 2021. cite arxiv:2103.14030Comment: The first 4 authors contribute equally. 3
- [16] Adam Paszke, Sam Gross, Francisco Massa, Adam Lerer, James Bradbury, Gregory Chanan, Trevor Killeen, Zeming Lin, Natalia Gimelshein, Luca Antiga, Alban Desmaison, Andreas Köpf, Edward Yang, Zach DeVito, Martin Raison, Alykhan Tejani, Sasank Chilamkurthy, Benoit Steiner, Lu Fang, Junjie Bai, and Soumith Chintala. Pytorch: An imperative style, high-performance deep learning library, 2019. cite arxiv:1912.01703Comment: 12 pages, 3 figures, NeurIPS 2019. 4
- [17] Olaf Ronneberger, Philipp Fischer, and Thomas Brox. U-net: Convolutional networks for biomedical image segmentation, 2015. cite arxiv:1505.04597Comment: conditionally accepted at MICCAI 2015. 2
- [18] Johannes L. Schönberger and Jan-Michael Frahm. Structure-from-motion revisited. In *CVPR*, pages 4104–4113. IEEE Computer Society, 2016. 4
- [19] Johannes L. Schönberger, Enliang Zheng, Jan-Michael Frahm, and Marc Pollefeys. Pixelwise view selection for unstructured multi-view stereo. In Bastian Leibe, Jiri Matas, Nicu Sebe, and Max Welling, editors, *ECCV (3)*, volume 9907 of *Lecture Notes in Computer Science*, pages 501–518. Springer, 2016. 4
- [20] Engin Tola, Christoph Strecha, and Pascal Fua. Efficient large-scale multi-view stereo for ultra high-resolution image sets. *Mach. Vis. Appl.*, 23(5):903–920, 2012. 4
- [21] Fangjinhua Wang, Silvano Galliani, Christoph Vogel, Pablo Speciale, and Marc Pollefeys. Patchmatchnet: Learned multi-view patchmatch stereo, 2021. 1, 5
- [22] Jiayu Yang, Wei Mao, Jose M. Alvarez, and Miaomiao Liu. Cost volume pyramid based depth inference for multi-view stereo. In *CVPR*, pages 4876–4885. IEEE, 2020. 1, 4, 5
- [23] Yao Yao, Zixin Luo, Shiwei Li, Tian Fang, and Long Quan. Mvsnet: Depth inference for unstructured multi-view stereo. In Vittorio Ferrari, Martial Hebert, Cristian Sminchisescu, and Yair Weiss, editors, *ECCV (8)*, volume 11212 of *Lecture Notes in Computer Science*, pages 785–801. Springer, 2018. 1, 4, 5
- [24] Yao Yao, Zixin Luo, Shiwei Li, Tianwei Shen, Tian Fang, and Long Quan. Recurrent mvsnet for high-resolution multi-view stereo depth inference. In *CVPR*, pages 5525–5534. Computer Vision Foundation / IEEE, 2019. 1, 4, 5
- [25] Zehao Yu and Shenghua Gao. Fast-mvsnet: Sparse-to-dense multi-view stereo with learned propagation and gauss-newton refinement. In *CVPR*, pages 1946–1955. IEEE, 2020. 4, 5